

# Fragmentation of spin-dipole strength in $^{90}\text{Zr}$ and $^{208}\text{Pb}$

T. Marketin<sup>a,b</sup>, E. Litvinova<sup>c</sup>, D. Vretenar<sup>b</sup>, P. Ring<sup>d</sup>

<sup>a</sup>*GSI Helmholtzzentrum für Schwerionenforschung, Planckstraße 1, D-64291 Darmstadt, Germany*

<sup>b</sup>*Physics Department, Faculty of Science, University of Zagreb, 10000 Zagreb, Croatia*

<sup>c</sup>*ExtreMe Matter Institute EMMI and Research Division, GSI Helmholtzzentrum für Schwerionenforschung, Planckstraße 1, D-64291 Darmstadt, Germany*

<sup>d</sup>*Physik-Department der Technischen Universität München, D-85748 Garching, Germany*

---

## Abstract

An extension of time-dependent covariant density functional theory that includes particle-vibration coupling is applied to the charge-exchange channel. Spin-dipole excitation spectra are calculated and compared to available data for  $^{90}\text{Zr}$  and  $^{208}\text{Pb}$ . A significant fragmentation is found for all three angular-momentum components of the spin-dipole strength as a result of particle-vibration coupling, as well as a shift of a portion of the strength to higher energy. A high-energy tail is formed in the strength distribution that linearly decreases with energy. Using a model-independent sum rule, the corresponding neutron skin thickness is estimated and shown to be consistent with values obtained at the mean-field level.

*Keywords:* covariant density functional theory, particle-vibration coupling, nuclear charge-exchange excitations

---

Spin-isospin excitations present a very active research topic both in nuclear structure and nuclear astrophysics. In particular, a detailed knowledge of the Gamow-Teller resonance, a collective oscillation of excess neutrons that coherently change the direction of their spin and isospin without changing

their orbital motion, is essential for understanding weak nuclear reactions involved in the process of nucleosynthesis, i.e.  $\beta$ -decay, electron and neutrino capture. Moreover, it has been shown that spin-dipole charge-exchange excitations, made up of three components with angular momentum and parity  $J^\pi = 0^-, 1^-$  and  $2^-$ , can significantly contribute to the total reaction rates and even compete with the contribution of Gamow-Teller transitions [1, 2, 3].

The spin-dipole strength can also provide information on basic properties of finite nuclei. The thickness of the neutron skin has been shown to constrain the neutron equation of state [4], and is also correlated with the nuclear symmetry energy [5]. While accurate data on the charge distribution in nuclei have been obtained by elastic electron scattering, our knowledge of neutron distribution comes primarily from hadron scattering, and the results are markedly model-dependent. Indirect methods for determining the neutron skin thickness have been proposed, based on energy differences between the Gamow-Teller and isobaric analogue resonances [6], and using the model-independent sum rule for the spin-dipole resonance [7]. Two recent  $(p, n)$  and  $(n, p)$  measurements of the spin-dipole response of  $^{90}\text{Zr}$  and  $^{208}\text{Pb}$  [8, 9] have also prompted new theoretical studies, in particular investigations based on the random phase approximation [10, 11, 12, 13].

Both measurements [8, 9] show a high-energy tail in the spin-dipole strength distribution that cannot be described by the simple one-particle – one-hole (1p1h) random phase approximation (RPA). Previous attempts to extend this framework using the 2p2h RPA were based on a non self-consistent approach that employs a phenomenological Woods-Saxon potential to obtain the ground-state wave functions [14]. In this Letter we in-

roduce a charge-exchange version of the particle-vibration coupling model based on time-dependent covariant density functional theory, and apply it to an analysis of spin-dipole strength distributions in  $^{90}\text{Zr}$  and  $^{208}\text{Pb}$ .

The basic quantity that describes small-amplitude motion of an even-even nucleus in an external field with frequency  $\omega$  is its response function  $R(\omega)$  [15]. It is obtained as a solution of the Bethe-Salpeter equation:

$$R(\omega) = \tilde{R}^0(\omega) + \tilde{R}^0(\omega)W(\omega)R(\omega), \quad (1)$$

where  $\tilde{R}^0(\omega)$  is the propagator of two uncorrelated quasiparticles in the static mean field, and the second term includes the in-medium nucleon-nucleon interaction  $W(\omega)$ . The two-body interaction  $W(\omega)$  contains static terms and a frequency-dependent term:

$$W(\omega) = V_\rho + V_\pi + V_{\delta\pi}^{LM} + \Phi(\omega) - \Phi(0). \quad (2)$$

$V_\rho$  and  $V_\pi$  represent the finite-range  $\rho$ -meson and  $\pi$ -meson exchange interactions, respectively. They are derived from the covariant energy density functional and read:

$$\begin{aligned} V_\rho(1, 2) &= g_\rho^2 \vec{\tau}_1 \vec{\tau}_2 (\beta\gamma^\mu)_1 (\beta\gamma_\mu)_2 D_\rho(\mathbf{r}_1, \mathbf{r}_2), \\ V_\pi(1, 2) &= \left(\frac{f_\pi}{m_\pi}\right)^2 \vec{\tau}_1 \vec{\tau}_2 (\boldsymbol{\Sigma}_1 \nabla_1) (\boldsymbol{\Sigma}_2 \nabla_2) D_\pi(\mathbf{r}_1, \mathbf{r}_2), \end{aligned} \quad (3)$$

where  $g_\rho$  and  $f_\pi$  are the coupling strengths,  $D_\rho$  and  $D_\pi$  are the meson propagators and  $\boldsymbol{\Sigma}$  is the generalized Pauli matrix [16]. The derivative type of the pion-nucleon coupling necessitates the inclusion of the zero-range Landau-Migdal term  $V_{\delta\rho}^{LM}$ , which accounts for the contact part of the nucleon-nucleon interaction [16].  $\Phi(\omega)$  describes the coupling of the quasiparticles to vibrations (phonons) generated by coherent nucleonic motion. In the quasiparticle

time blocking approximation (QTBA) [17] it can be written in the following operator form:

$$\Phi(\omega) = \sum_{m,\eta} g_m^{(\eta)\dagger} \tilde{R}^{0(\eta)}(\omega - \eta\omega_m) g_m^{(\eta)}, \quad (4)$$

where the index  $m$  enumerates vibrational modes with frequencies  $\omega_m$  and coupling amplitude matrices  $g_m^{(\eta)}$ , and the index  $\eta = \pm 1$  denotes forward and backward components. In Eq. (2) the term  $\Phi(0)$  is subtracted to remove the effect of double counting the phonon coupling, because the parameters of the density functional have been adjusted to ground-state data and, therefore, already include essential static phonon contributions. The energy-dependent effective interaction of Eq. (4) leads to fragmentation of nuclear spectra and determines the width of giant resonances [18].

The strength function  $S(\omega)$ :

$$S(E, \Delta) = -\frac{1}{\pi} \text{Im} \langle P^\dagger R(E + i\Delta) P \rangle, \quad (5)$$

yields the spectral distribution of the nuclear response in a given external field  $P$ . The field operators for charge-exchange spin-dipole transitions read:

$$P_\pm^\lambda = \sum_i r(i) [\boldsymbol{\sigma}(i) \otimes Y_1(i)]_\lambda t_\pm(i), \quad (6)$$

where  $t_\pm$  denotes the isospin raising and lowering operators.

The phonon coupling terms augment the RPA spectrum with additional p-h $\otimes$ phonon components that generally lead to significant fragmentation of giant resonances [18]. In Fig. 1 we compare the spin-dipole strength distribution in  $^{90}\text{Zr}$  calculated using the relativistic random phase approximation (RRPA), and the relativistic time-blocking approximation (RTBA). In both

models the NL3 [19] relativistic mean-field effective interaction has consistently been used for the calculation of the mean-field ground-state, the RPA phonons, and the spin-dipole charge-exchange excitations.

The prominent RRPA peaks (dashed curves) disappear when particle-vibration coupling is included in the RTBA (solid curves). In the  $t_-$  channel, for instance, only a broad resonance remains with the peak at 23.5 MeV, in very good agreement with available data [8]. The three angular-momentum components do not, however, follow the energy hierarchy  $E(2^-) < E(1^-) < E(0^-)$  predicted by recent Skyrme-RPA calculations [10, 11]. While the RTBA predicts the  $2^-$  component to be the lowest one with the centroid energy  $m_1^{2^-} / m_0^{2^-} = 25.4$  MeV,  $0^-$  is found to be lower than the  $1^-$  component, with centroid energies at 29.4 MeV and 32.6 MeV, respectively. This is probably due to the fact that the exchange terms are neglected in the mean-field calculation. Namely, as shown in a recent study [12], a fully consistent relativistic Hartree-Fock (RHF) + RPA calculation yields  $E(2^-) < E(1^-) < E(0^-)$  for the excitation energies of spin-dipole components.

The inclusion of particle-vibration coupling leads to a shift of the strength to higher excitation energies. A high-energy tail is formed in the region above 30 MeV where the strength decreases almost linearly with increasing energy, in close agreement with experimental results. In contrast, the RRPA strength decreases more rapidly above 30 MeV, and becomes 5 to 10 times smaller than the experimental strength above 40 MeV.

In the  $t_+$  channel the two dominant peaks predicted by the RRPA merge into a single broad structure that extends up to approximately 15 MeV excitation energy. The tail at higher energies decreases approximately linearly

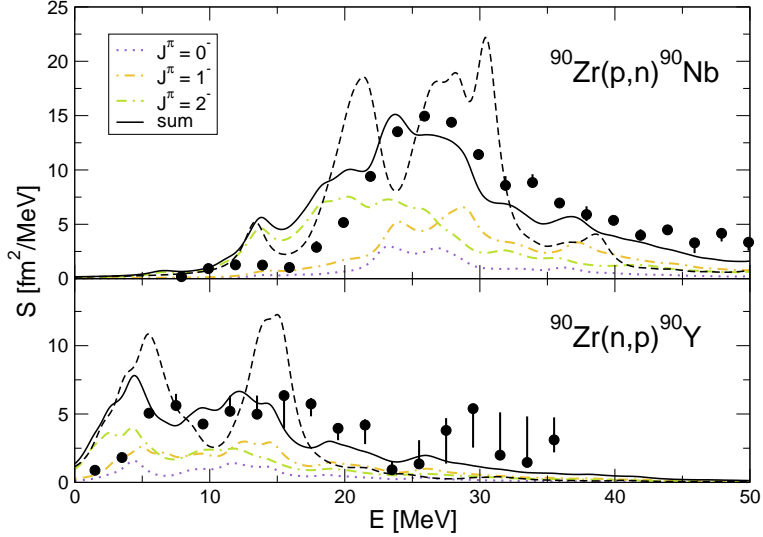


Figure 1: Spin-dipole strength distributions for the  $t_-$  (upper panel) and the  $t_+$  (lower panel) channels in  $^{90}\text{Zr}$ . On the horizontal axis the excitation energy is plotted with respect to the ground state of  $^{90}\text{Zr}$ . The solid black curve represents the sum of the strength distributions of the  $0^-$ ,  $1^-$  and  $2^-$  components, calculated in the RTBA that includes particle-vibration coupling. The dashed black curves denotes the corresponding RRPA strength function. In both cases the imaginary part of the energy is set to  $\Delta = 1$  MeV. The experimental results denoted by full circles are from Ref. [8].

with increasing energy. One might notice a very good agreement with data, except in the low-energy region below 5 MeV, where both the RRPA and the RTBA predict spin-dipole strength, originating predominantly from the  $2^-$  component, that is considerably larger than the measured distribution.

The results for the spin-dipole strength in  $^{208}\text{Pb}$  are shown in Fig. 2. The data exhibit a broad asymmetric resonance centered at 25 MeV, and an additional small peak at approximately 6 MeV. The RTBA results reproduce these structures, even though the calculated width of the main resonance is

slightly larger than the empirical value. As in the previous case, a portion of the strength is shifted to higher energies by the inclusion of particle-vibration coupling, in very good agreement with data above 35 MeV. Obviously in this region the RRPA strength distribution decreases much faster with energy compared to RTBA. The ordering of the angular-momentum components of the strength is the same as in the case of  $^{90}\text{Zr}$ :  $E(2^-) < E(0^-) < E(1^-)$ . The lower panel of Fig. 2 displays the distributions of the  $\text{SD}_+$  strength. In this case the strength is concentrated in a single peak centered at 7.5 MeV. Relatively little fragmentation is obtained in comparison with the RRPA results, even though some strength is shifted to higher excitation energy in the RTBA. These findings are supported by the available data from Ref. [20], where a single peak has been observed at approximately 7.5 MeV excitation energy.

In the case of  $^{208}\text{Pb}$  data are also available for each component of the spin-dipole strength [9]. In Fig. 3 we display a comparison between the RRPA, RTBA and the experimental results for  $J^\pi = 0^-, 1^-$  and  $2^-$ . The RRPA predicts that the strength of the  $0^-$  component is concentrated in a single peak at the excitation energy of  $\approx 28$  MeV with respect to the ground state of  $^{208}\text{Pb}$ . Particle-vibration coupling induces fragmentation and spreading of this strength, but the basic structure of the distribution is not altered. Obviously this does not completely agree with the experimental results. For the  $1^-$  components the main peak is centered around 30 MeV, whereas the experiment places it around 23 MeV. The opposite situation occurs for the  $2^-$  component, for which the calculated distribution is in qualitative agreement with experiment, even though the centroid of the main peak is calculated

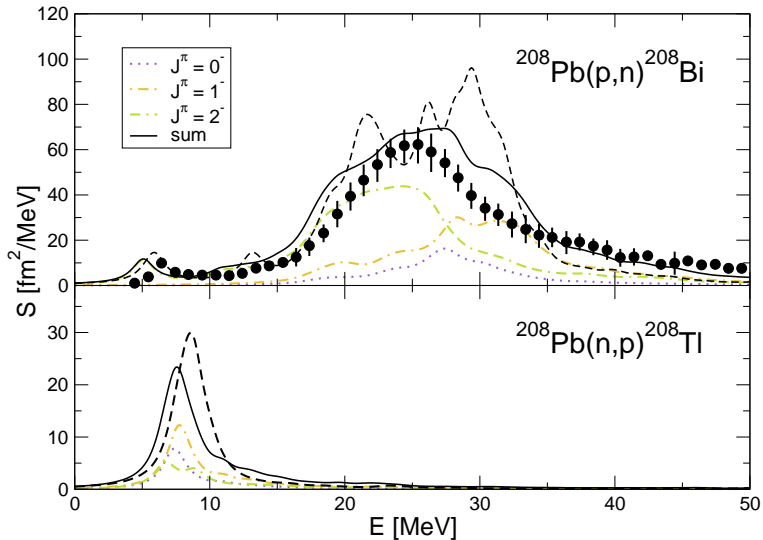


Figure 2: Same as described in the caption to Fig. 1 but for  $^{208}\text{Pb}$ . The data are from Ref. [9].

few MeV below the measured resonance. In Ref. [13] the results have been brought in agreement with experiment by the inclusion of tensor correlations in the Skyrme energy density functional. These correlations exhibit a multipole-dependent effect on spin-dipole excitations. It is interesting to note that in this case experimental results indicate that the  $1^-$  component of the spin-dipole resonance is actually below the  $2^-$  component.

Using the calculated strength distributions, we have also determined the sum-rule values for the spin-dipole response of  $^{90}\text{Zr}$  and  $^{208}\text{Pb}$ . The model independent sum rule relates the spin-dipole strength to the neutron and proton ground-state radii [21]:

$$S_-^\lambda - S_+^\lambda = \frac{2\lambda + 1}{4\pi} \left( N \langle r^2 \rangle_n - Z \langle r^2 \rangle_p \right), \quad (7)$$

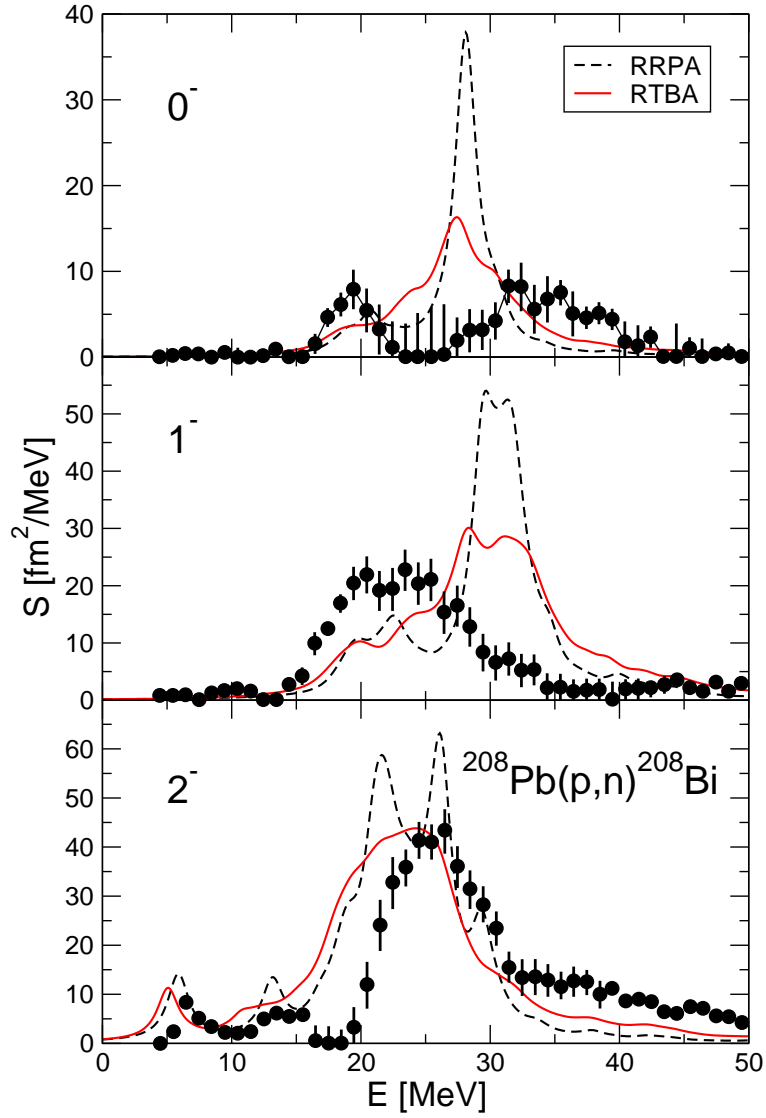


Figure 3: Spin-dipole strength distributions in  $^{208}\text{Pb}$  for the  $J^\pi = 0^-, 1^-$  and  $2^-$  components. The black dashed curves are the RRPA results, and the solid red curves denote results obtained with the particle-vibration coupling model. Data are from Ref. [9].

Table 1: Spin-dipole sum-rule values, proton and neutron *rms* radii, and thickness of the neutron skin of  $^{90}\text{Zr}$  and  $^{208}\text{Pb}$ . The proton radii correspond to the self-consistent ground-state distributions, whereas the neutron radii are calculated using the sum rule of Eq. (7). Sum rules are given in units of  $\text{fm}^2$ , and radii in fm. Error estimates in the experimental value of the sum rule arise from statistical, systematic and multipole decomposition uncertainties, respectively.

	$^{90}\text{Zr}$	$^{208}\text{Pb}$
$S_- - S_+$ (g.s.)	160.925	1222.044
$S_- - S_+$ (calc.)	160.963	1213.562
$S_- - S_+$ (exp.)	$148 \pm 6 \pm 7 \pm 7$ [8]	
$\sqrt{\langle r^2 \rangle_p}$ (g.s.)	4.193	5.459
$\sqrt{\langle r^2 \rangle_n}$ (calc.)	4.308	5.731
$\sqrt{\langle r^2 \rangle_n}$ (exp.)	$4.26 \pm 0.04$ [8]	
$\delta_{np}$ (calc.)	0.115	0.272
$\delta_{np}$ (exp.)	$0.07 \pm 0.04$ [8]	$0.083 < \delta_{np} < 0.111$ [25]
		$0.156^{+0.025}_{-0.021}$ [27]
		$0.19 \pm 0.09$ [23]

where  $S_{\pm}^{\lambda}$  denotes the total SD strength in the  $t_{\pm}$  channel for angular momentum  $\lambda$ .  $S_{\pm}$  will denote the sum of spin-dipole strengths of the three components. The neutron skin thickness  $\delta_{np}$  is defined as the difference of neutron and proton *rms* radii:

$$\delta_{np} = \sqrt{\langle r^2 \rangle_n} - \sqrt{\langle r^2 \rangle_p}. \quad (8)$$

The results obtained in the present study are summarized in Table 1. The

first and second rows of the table give the values of the sum rule obtained employing the self-consistent ground-state mean-field solutions and the calculated SD strengths, respectively. The experimental value of the sum rule for  $^{90}\text{Zr}$  [8] is shown in the third row. The difference between the two theoretical results is very small because the model is self-consistent, but they both overestimate the experimental value. The radii of proton distributions in the fourth row are extracted from the self-consistent ground-state densities, and these values are in excellent agreement with data [22]. In the fifth and sixth rows we include the *rms* radii of neutron distributions in  $^{90}\text{Zr}$  and  $^{208}\text{Pb}$ , calculated from Eq. (7) using the proton ground-state radii and the calculated SD strength distributions, and the experimental value for  $^{90}\text{Zr}$ , respectively. Finally, the calculated and experimental values for the neutron skin thickness are given in the last two rows of Table 1.

For  $^{90}\text{Zr}$  the calculated sum rule is 9% larger than the measured value. This leads to a neutron rms radius  $\sqrt{\langle r^2 \rangle_n} = 4.308$  fm, and neutron skin thickness  $\delta_{np} = 0.115$  fm, both at the upper limit of the experimental error bars. We note that the relativistic Hartree-Fock + RPA calculation predicts the neutron skin thickness  $\delta_{np} = 0.092$  fm [12], while Skyrme-based results range from  $\delta_{np} = 0.055$  fm to  $\delta_{np} = 0.106$  fm [10].

There are no experimental values of the total spin-dipole strength in  $^{208}\text{Pb}$ , but several measurements of the neutron skin thickness have been reported. A comparison of the measured cross section for the isoscalar giant dipole resonance and the DWBA calculation yielded the neutron skin thickness  $\delta_{np} = 0.19 \pm 0.09$  fm [23]. Microscopic optical potential analyses of intermediate energy elastic proton scattering give  $\delta_{np} \approx 0.17$  fm [24], and

$0.083 \text{ fm} < \delta_{np} < 0.111 \text{ fm}$  [25]. Using the correlation between neutron skin thickness and the isovector dipole polarizability obtained with the Skyrme functional [26], the very recent results on polarized proton inelastic scattering at forward angles yield the value  $\delta_{np} = 0.156_{-0.021}^{+0.025} \text{ fm}$  [27]. The value obtained from the calculated SD sum rule in the present study is  $\delta_{np} = 0.272 \text{ fm}$ , considerably larger than the empirical values. The RHF + RPA model predicts  $\delta_{np} = 0.234 \text{ fm}$  [12], and values obtained from various Skyrme-based models range between  $\delta_{np} = 0.125 \text{ fm}$  and  $\delta_{np} = 0.228 \text{ fm}$  [10]. The relatively large neutron skin thickness that we have obtained in the present study is peculiar to the relativistic effective interaction NL3 [19], characterized by a large asymmetry energy. Employing one of the modern relativistic functionals with non-linear effective interactions in the isovector channel and lower asymmetry energy as, for instance, DD-PC1 [28], the thickness of ground-state neutron skin is calculated:  $\delta_{np} = 0.088 \text{ fm}$  for  $^{90}\text{Zr}$ , and  $\delta_{np} = 0.201 \text{ fm}$  for  $^{208}\text{Pb}$ . This type of functionals, however, has not yet been implemented in the RTBA model used in this study.

In summary, the first calculation of charge-exchange spin-dipole excitations in  $^{90}\text{Zr}$  and  $^{208}\text{Pb}$ , using the particle-vibration coupling model based on the covariant density functional theory, is reported. Compared to the RRPA results, the RTBA model for particle-vibration coupling leads to pronounced fragmentation of the strength distribution for all three angular-momentum components of the spin-dipole operator. A portion of the strength is shifted to higher excitation energy, and the corresponding shift of the centroid energy is 2.5 MeV for  $^{90}\text{Zr}$ , and 1 MeV for  $^{208}\text{Pb}$ . As a result of particle-vibration coupling a high-energy tail of the strength distribution is formed and the

strength in this region decreases almost linearly with increasing energy, in close agreement with data. Furthermore, a model-independent SD sum rule has been used to determine the neutron *rms* radii and the thickness of the neutron skin. The calculated skin thickness  $\delta_{np} = 0.115$  fm for  $^{90}\text{Zr}$  and  $\delta_{np} = 0.272$  fm for  $^{208}\text{Pb}$ , are larger than the available empirical values, and reflect the high asymmetry energy of the particular relativistic energy density functional used in the present study.

## ACKNOWLEDGMENTS

This work was supported in part by the Helmholtz International Center for FAIR within the framework of the LOEWE program launched by the State of Hesse, the Alliance Program of the Helmholtz Association (HA216/EMMI), and by the MZOS - project 1191005-1010.

## References

- [1] E. Kolbe and K. Langanke, Phys. Rev. C 63, 025802 (2001).
- [2] T. Suzuki and H. Sagawa, Nucl. Phys. A 718, 446 (2003).
- [3] N. Paar, D. Vretenar, T. Marketin, and P. Ring, Phys. Rev. C 77, 024608 (2008).
- [4] S. Typel and B. A. Brown, Phys. Rev. C 64, 027302 (2001).
- [5] S. Yoshida and H. Sagawa, Phys. Rev. C 73, 044320 (2006).
- [6] D. Vretenar, N. Paar, T. Nikšić, and P. Ring, Phys. Rev. Lett. 91, 262502 (2003).

- [7] A. Krasznahorkay *et al.*, Phys. Rev. Lett 82, 3216 (1999).
- [8] K. Yako, H. Sagawa, and H. Sakai, Phys. Rev. C 74, 051303(R)(2006).
- [9] T. Wakasa, arXiv:1004.5220.
- [10] H. Sagawa, S. Yoshida, X. Zhou, K. Yako, and H. Sakai, Phys. Rev. C 76, 024301 (2007).
- [11] S. Fracasso and G. Colò, Phys. Rev. C 76, 044307 (2007).
- [12] H. Liang, N. Van Giai, and J. Meng, Phys. Rev. Lett. 101, 122502 (2008).
- [13] C. L. Bai, H. Q. Zhang, H. Sagawa, X. Z. Zhang, G. Colò, and F. R. Xu, Phys. Rev. Lett. 105, 072501 (2010).
- [14] S. Drożdż, F. Osterfeld, J. Speth, and J. Wambach, Phys. Lett. B 189, 271 (1987).
- [15] P. Ring and P. Schuck, *The Nuclear Many-body Problem* (Springer Verlag, Heidelberg, 1980).
- [16] N. Paar, T. Nikšić, D. Vretenar, and P. Ring, Phys. Rev. C 69, 054303 (2004).
- [17] V.I. Tselyaev, Phys. Rev. C 75, 024306 (2007).
- [18] E. Litvinova, P. Ring, and V. Tselyaev, Phys. Rev. C 75, 064308 (2007).
- [19] G. A. Lalazissis, J. König, and P. Ring, Phys. Rev. C 55, 540 (1997).
- [20] S. A. Long *et al.*, Phys. Rev. C 57, 3191 (1998).

- [21] C. Gaarde *et al.*, Nucl. Phys. A 369, 258 (1981).
- [22] H. de Vries, C. W. de Jager, and C. de Vries, At. Data Nucl. Data Tables 36, 495 (1987).
- [23] A. Krasznahorkay *et al.*, Nucl. Phys. A 567, 521 (1994).
- [24] S. Karataglidis, K. Amos, B. A. Brown, and P. K. Deb, Phys. Rev. C 65, 044306 (2002).
- [25] B. C. Clark, L. J. Kerr, and S. Hama, Phys. Rev. C 67, 054605 (2003).
- [26] P.-G. Reinhard and W. Nazarewicz, Phys. Rev. C 81, 051303(R) (2010).
- [27] A. Tamii *et al.* Phys. Rev. Lett. 107, 062502 (2011).
- [28] T. Nikšić, D. Vretenar, and P. Ring., Phys. Rev. C 78, 034318 (2008).